Correlation between microstructural and magnetic properties of Tb implanted ZnO

P. P. Murmu, J. Kennedy, B. J. Ruck, G. V. M. Williams, A. Markwitz et al.

Citation: AIP Conf. Proc. **1525**, 300 (2013); doi: 10.1063/1.4802337
View online: http://dx.doi.org/10.1063/1.4802337
View Table of Contents: http://proceedings.aip.org/dbt/dbt.jsp?KEY=APCPCS&Volume=1525&Issue=1
Published by the American Institute of Physics.

Correlation Between Microstructural and Magnetic Properties of Tb Implanted ZnO

P. P. Murmu [a,b,c], J. Kennedy [a,b], B. J. Ruck [b,c], G. V. M. Williams [b,c], A. Markwitz[a,b], S. Rubanov [d] and A. A. Suvorova [e]

[a]*National Isotope Centre, GNS Science, PO Box 31312, Lower Hutt 5010, New Zealand*
[b]*The MacDiarmid Institute for Advanced Materials and Nanotechnology, New Zealand*
[c]*School of Chemical and Physical Sciences, Victoria University of Wellington, PO Box 600, Wellington 6140, New Zealand*
[d]*University of Melbourne, Bio21 Institute, Melbourne, Vic. 3010, Australia*
[e]*Centre for Microscopy, Characterization and Analysis, The University of Western Australia, Crawley, 6009 Western Australia, Australia*

Abstract. We report the results from microstructural and magnetic measurements on 40 keV Tb implanted ZnO single crystals. RBS and channeling measurements for 6.7×10^{14} cm^{-2} implanted ZnO showed that around 85% of the Tb atoms occupied Zn substitutional lattice sites. Annealing at 650 ^{o}C had a small effect on the Tb location where only 81% of the Tb atoms were located at substitutional lattice sites. Energy-filtered TEM micrographs showed that the Tb atoms were located at an average depth of ~15 nm. Raman spectroscopy results indicated that annealing resulted in a reduction in the implantation induced disorder in the ZnO lattice. Room temperature ferromagnetic order was observed in ZnO:Tb annealed at 650 ^{o}C. Superparamagnetic behavior was observed with an average blocking temperature of ~40 K for high Tb concentrations and a distribution in the blocking temperature for low Tb concentrations.

Keywords: DMS, ZnO, terbium, implantation, RBS and channeling.
PACS: 68.37, 74.25.nd, 75.20.-g, 75.50.Dd

INTRODUCTION

Dilute magnetic semiconductors (DMSs) are a group of materials with potential to revolutionize the semiconductor industry and lead to applications that include integrated electronic and magnetic memory [1]. Wide band gap semiconductors GaN and ZnO have attracted significant attention due to the predicted room temperature ferromagnetism [2]. ZnO has several advantages over GaN which include large exciton binding energy (~60 meV) as compared to ~25 meV for GaN, better radiation resistance and availability of high quality substrates. This has led to increased reports from experimental studies that are primarily focused on transition metal doped ZnO [3]. A report of very high magnetic moment (4000 μ_B per ion) in gadolinium (Gd) doped GaN [4] resulted in increased studies of rare-earth (RE) elements as a potential source of magnetism in DMSs. Potzger *et al.* [5] reported ferromagnetic order in ZnO single crystals which has stimulated research into the use of rare-earths in ZnO to produce DMSs.

The origin of ferromagnetic order in DMS systems is often debatable. Ferromagnetic order has been reported in various RE doped ZnO systems such as ZnO:Ce [6], ZnO:Nd [7], ZnO:Eu [8], ZnO:Gd [5, 9, 10], ZnO:Tb [11, 12], and ZnO:Er [13]. However, Ney *et al.* [14] only observed paramagnetic behavior from isolated Gd ions contrary to ferromagnetism observed in ZnO:Gd [5, 10], and the authors supported their experimental results with DFT calculations. They reported that the Gd atoms are more likely to aggregate at interstitials as the doping concentration increases. This can lead to phase separation and segregation that can affect the magnetic properties. For example, Zhou *et al.* reported ferromagnetic order in Tb implanted ZnO single crystals originating from Tb-nanoclusters [11]. Monteiro *et al.* reported that Tb is less likely to occupy substitutional lattice sites when compared with Tm and Er [15]. In this paper, we present the results from microstructural and magnetic measurements on Tb implanted ZnO.

EXPERIMENTAL PROCEDURE

40 keV Tb ions were implanted into commercially available hydrothermally grown ZnO (0001) from Semi-Wafer Inc. using a low energy ion implanter

Application of Accelerators in Research and Industry
AIP Conf. Proc. 1525, 300-304 (2013); doi: 10.1063/1.4802337

[16]. The implanted Tb fluences ranged from 6.7 × 10^{14} to 1.1 × 10^{16} cm^{-2} resulting in 0.7 to 7.4 at.% Tb in the near surface region of ZnO. DYNAMIC-TRIM [17] calculations show an average implantation depth of 12 nm and maximum depth of 25 nm. The implanted samples were subsequently annealed at 650 ^{o}C in a vacuum chamber for 30 minutes with a base pressure of 1x10^{-7} mbar. Transmission electron microscopy (TEM) measurements were made to probe the microstructure and elemental composition. Rutherford backscattering spectrometry and channeling (RBS/C) analyses were carried out to estimate the crystalline quality after implantation and annealing using a collimated 2 MeV He^{+} beam [18]. Structural modifications before and after annealing were investigated at ambient temperature using a Jobin-Yvon LabRam micro-Raman system. An Ar^{+} laser with a wavelength of 514 nm was used as the excitation source and the spectra were collected in the backscattering geometry with a liquid nitrogen cooled charge coupled device detector. A Quantum Design superconducting quantum interference device (SQUID) was employed to study the magnetic properties of the films.

Results and Discussions

The effect of Tb implantation and annealing on the ZnO crystal structure was assessed using RBS/C. Figure 1 shows random and [0001]-aligned RBS spectra for 6.7 × 10^{14}, 3.9 × 10^{15} and 1.1 × 10^{16} Tb cm^{-2} implanted and 650 ^{o}C annealed ZnO single crystals.

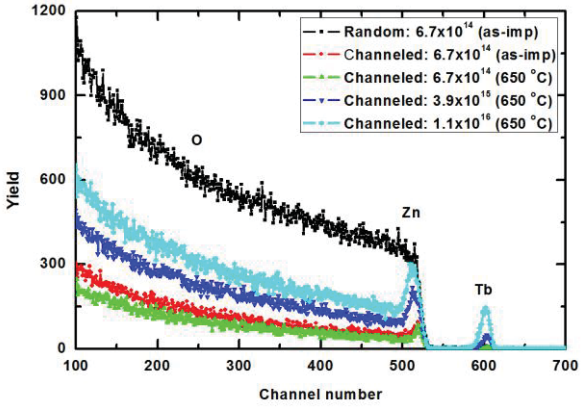

FIGURE 1. Random and [0001]-aligned RBS spectra for 6.7 × 10^{14}, 3.9 × 10^{15} and 1.1 × 10^{16} Tb cm^{-2} implanted and 650 ^{o}C annealed ZnO single crystals.

The 6.7 × 10^{14} Tb cm^{-2} as-implanted ZnO sample showed $^{Zn}\chi_{min}$ ~ 16%, which reduced to ~ 12% upon annealing at 650 ^{o}C. $^{Zn}\chi_{min}$ for 3.9 × 10^{15} and 1.1 × 10^{16} Tb cm^{-2} implanted and 650 ^{o}C annealed ZnO was ~ 27% and ~ 36%, respectively. Low $^{Zn}\chi_{min}$ values indicate moderate implantation induced disorder in the ZnO lattice.

Angle dependent scans around the [0001] axis were made to probe the incorporation of Tb atoms into the ZnO lattice. Angular scan profiles for Zn and Tb for 6.7 × 10^{14}, 3.9 × 10^{15}, and 1.1 × 10^{16} Tb cm^{-2} implanted and 650 ^{o}C annealed ZnO single crystals are shown in Fig. 2. Zn and Tb angular scans show a similar trend, suggesting that they have similar disorder. The angular scans show characteristics of substitutional disorder. The fraction of Tb atoms located in substitutional sites was estimated from (1 - $^{Tb}\chi_{min}$) / (1 - $^{Zn}\chi_{min}$), where $^{Tb}\chi_{min}$ and $^{Zn}\chi_{min}$ are χ_{min} for Tb and Zn, respectively. In 6.7 × 10^{14} Tb cm^{-2} as-implanted ZnO, around 85% of the Tb atoms occupy substitutional lattice sites. Upon annealing at 650 ^{o}C the fraction of Tb atoms at substitutional lattice sites decreased to ~81%. Around 46.5% Tb atoms were found to reside at the substitutional lattice sites for a 3.9 × 10^{15} Tb cm^{-2} implanted and 650 ^{o}C annealed ZnO single crystal. For 1.1 × 10^{16} Tb cm^{-2} implanted around 29.4% and 20.6% Tb atoms were estimated to occupy the substitutional lattice sites for as-implanted and 650 ^{o}C annealed ZnO, respectively.

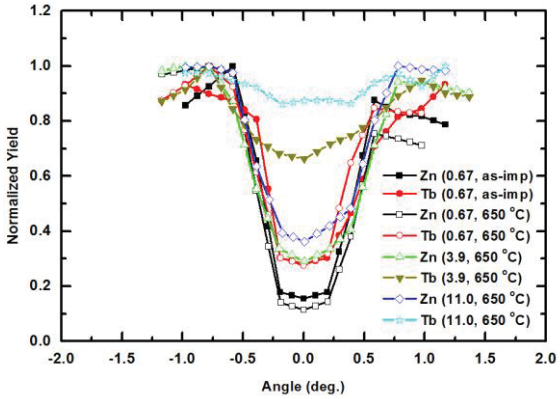

FIGURE 2. Angular scans along the [0001]-direction measured for Tb implanted and 650 ^{o}C annealed ZnO single crystals. Fluences are shown in the bracket with a unit of 10^{15} ions cm^{-2} along with the annealing conditions.

The RBS/C results for Tb fluences 6.7 × 10^{14} ions cm^{-2} are different from those observed when Gd is implanted into ZnO. For example, in as-implanted ZnO:Gd almost 100% [19] of the atoms occupy substitutional lattice sites, whereas in ZnO:Tb only 85% of the Tb atoms were found at substitutional sites. Annealing has a profound effect on ZnO:Gd and it resulted in around 78% of the Gd atoms residing at substitutional lattice sites. In ZnO:Tb, annealing had a small effect where the fraction of substitutional Tb

atoms decreased from 85% to 81%. Miranda *et al.* [20] reported that the rapid thermal annealing of Pr and Eu into ZnO epitaxial layers resulted in out-diffusion of rare-earth atoms into random interstitials which are likely to form clusters. The small reduction in the fraction of Tb atoms in substitutional lattice sites after annealing suggests that annealing is unlikely to induce a major re-arrangement of Tb atoms, however, the formation of Tb nanoparticles cannot be completely overruled. The site location of some other rare earth atoms in ZnO was reported by Monteiro *et al.* [15] where they found that Tm and Er in ZnO predominantly occupy substitutional lattice sites, which was not the case for Eu and Tb in ZnO.

Scanning Transmission Electron Microscopy (STEM) and Energy-filtered TEM (EFTEM) micrographs were obtained to investigate the microstructural properties of Tb implanted ZnO. Figure 3 shows a high-angle annular dark-field imaging (HAADF) STEM and elemental maps for Tb, Zn (jump-ratio) and O for a 3.9×10^{15} Tb cm^{-2} implanted and 650 ^{o}C annealed ZnO single crystal. The jump-ratio is an elemental map obtained from the ratio of two images recorded by selecting before and after ionization edge of the element of interest. The HAADF-STEM image shows that the implanted region is up to ~ 25 nm as shown in the Fig. 3(a). The HAADF-STEM is particularly useful to identify the high Z elements in light matrix and can distinctly be used to identify Tb atoms in ZnO matrix. The EFTEM micrograph in Fig. 3(b) shows that the Tb atoms are primarily located in the implantation region at an average depth of 15 nm. The Zn jump-ratio in Fig. 3(c) shows a uniform Zn distribution across the layer. The Tb EFTEM micrograph in Fig. 3(b) suggests that there are Tb-rich clusters similar to those observed in Gd implanted and annealed ZnO [10].

The structural properties of Tb implanted ZnO were further characterized by Raman spectroscopy. The Raman spectra obtained for un-implanted, 6.7×10^{14}, 3.9×10^{15} and 1.1×10^{16} Tb cm^{-2} implanted and 650 ^{o}C annealed ZnO single crystals are shown in Fig. 4. All samples exhibit strong E_2(high) peaks originating from wurtzite ZnO. The $2E_2$(M) Raman peaks are attributed to second order scattering in ZnO.

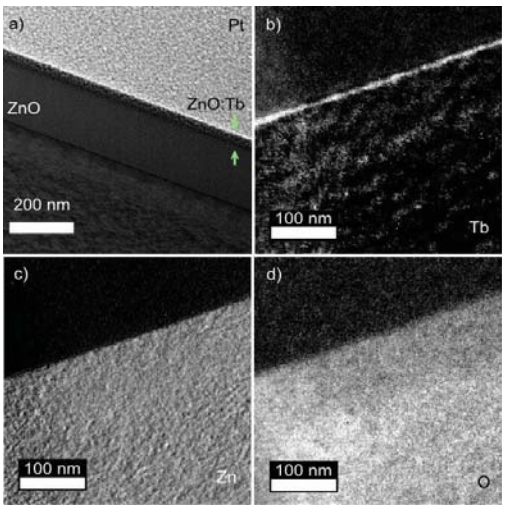

FIGURE 3. (a) HAADF-STEM and EFTEM elemental maps for (b) Tb (c) Zn (jump-ratio) and (d) O for a 3.9×10^{15} Tb cm^{-2} implanted and 650 ^{o}C annealed ZnO single crystal.

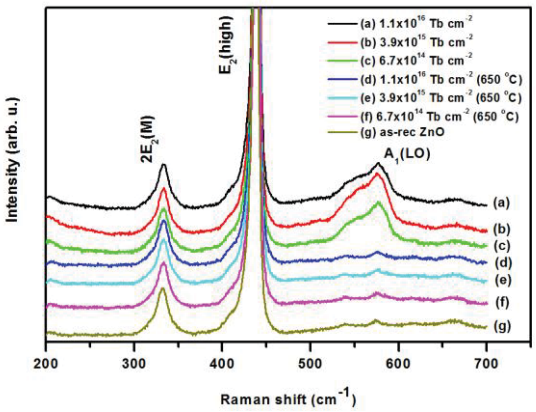

FIGURE 4. Raman spectra of as-received, and Tb implanted and 650 ^{o}C annealed ZnO single crystals.

A broad peak from 520 to 600 cm^{-1} with distinct peaks at around 576 cm^{-1} is observed in all as-implanted ZnO:Tb samples (see Fig. 4(a)-(c)). The Raman peaks at around 576 cm^{-1} are attributed to the ZnO A_1(LO) mode. The broad peaks in the 520 to 600 cm^{-1} region were significantly reduced after annealing as can be seen in Fig. 4(d) where annealing leads to spectra that are similar to un-implanted ZnO. Figures 4(d)-(f) suggest that the annealing of the ZnO:Tb samples at 650 ^{o}C leads to recovery of the implantation induced disorders in ZnO matrix. Similar behavior was also observed in Gd implanted ZnO single crystals [19]. Broad peaks in the 520 to 600 cm^{-1} region are often reported in ion implanted ZnO [21-23] and they appear to match the phonon DOS in disordered ZnO. Furthermore, intrinsic defects, mainly

oxygen vacancies, are believed to enhance the Raman scattering from the whole Brillouin zone, and the A_1(LO) peak is believed to be enhanced by resonant Raman scattering [22].

The field dependent magnetization from 6.7×10^{14}, 3.9×10^{15} and 1.1×10^{16} Tb cm^{-2} implanted and 650 ^{o}C annealed ZnO single crystals are presented in Fig. 5. Ferromagnetic order is clearly observed in these samples. We note that there was no evidence for ferromagnetic order in the unannealed crystals, which shows that annealing at 650 ^{o}C is required to induce ferromagnetic order. The high field magnetization, M_S, at 5 K for 6.7×10^{14}, 3.9×10^{15} and 1.1×10^{16} Tb cm^{-2} implanted and annealed ZnO:Tb was found to be around 40×10^{-4}, 18×10^{-4} and 12×10^{-4} emu/cm^3, respectively, where magnetic moments were divided by the substrate volume with coercive fields of ~300 Oe. Field dependent magnetization measurements at 300 K (not shown) showed that the ferromagnetic ordering temperature is above 300 K.

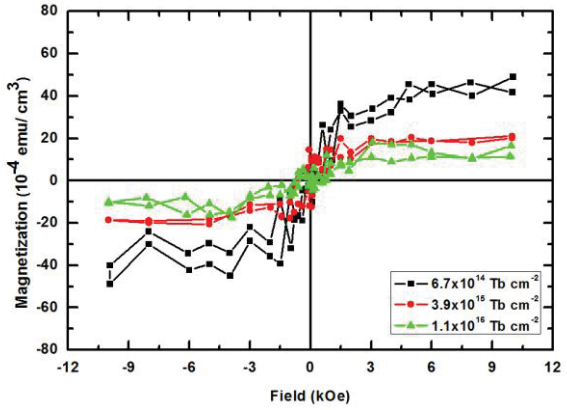

FIGURE 5. M(H) curves for Tb implanted and 650 ^{o}C annealed ZnO single crystals. SQUID measurements were performed at 5 K.

The low field temperature dependent magnetization data for the 3.9×10^{15} and 1.1×10^{16} Tb cm^{-2} implanted and 650 ^{o}C annealed ZnO samples are shown in Fig. 6. The zero-field-cooled (ZFC) magnetization from the 1.1×10^{16} Tb cm^{-2} implanted and annealed ZnO crystal increases with increasing temperature up to ~40 K and then it decreases and the ZFC and field-cooled (FC) magnetization data overlap above ~40 K. The FC and ZFC results indicate that superparamagnetic behavior occurs in ZnO:Tb and it arises from small nanoparticles where the blocking temperature is ~40 K. The FC magnetization data continues to increase below ~40 K and this can be attributed to paramagnetism from isolated Tb ions. The ZFC and FC data from the 3.9×10^{15} and implanted and 650 ^{o}C annealed ZnO crystal shows similar behavior. However, in this case the ZFC and FC curves separate at ~300 K, which indicates that there is a distribution in the nanoparticle sizes and this leads to a distribution in the blocking temperature.

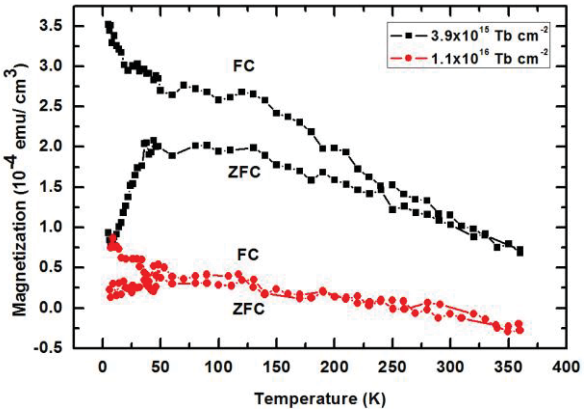

FIGURE 6. FC and ZFC magnetization curves for Tb implanted and 650 ^{o}C annealed ZnO single crystals. The applied magnetic field was 100 Oe.

The superparamagnetic behavior observed after Tb implantation and annealing is unlikely to arise from Tb, Tb_2O_3 or TbZn nanoparticles. This is because Tb has a Curie temperature of 237 K [24], Tb_2O_3 has a Neel temperature of between 2 K and 7 K [25, 26] and TbZn has a Curie temperature of ~204 K [27]. All of these temperatures are below the ferromagnetic ordering temperature of >300 K that we observed after Tb implantation and annealing. However, small nanoparticles from other Tb-rich complexes can also contribute towards superparamagnetism around 300 K. Wu *et al.* [12] also reported room temperature ferromagnetism in polycrystalline Tb doped ZnO films, which they attributed to defects present in the films. Other studies on ZnO have reported that the ferromagnetic order is related to Zn vacancies [28, 29]. Our results suggest that the superparamagnetism in Tb implanted and annealed ZnO crystals could be due to clusters of point detects. Similar trend was also observed in Gd implanted and annealed ZnO [30], which implies that Gd or Tb compounds are less likely to give rise the ferromagnetism in our samples. Carrier mediated exchange mechanism [2] appears to be a likely mechanism for room temperature ferromagnetic order observed in Tb implanted and annealed ZnO. The RBS/C results suggest that for low fluences implanted ZnO the majority of Tb atoms are located at substitutional lattice sites even after annealing the samples at 650 ^{o}C. A long range exchange interaction can occur in substitutionally located Tb ions as proposed for DMS systems [2]. The origin of room temperature ferromagnetic order in ZnO:Tb remains rather unclear and is often assigned to the defects

present in ZnO films [11, 12]. It requires further investigations using powerful characterization techniques such as synchrotron XRD, element specific X-ray magnetic circular dichroism (XMCD) and ferromagnetic resonance (FMR) in order to elucidate the ferromagnetism in ZnO:Tb.

In summary, RBS/C results showed that around 85% of the Tb atoms occupy substitutional lattice sites in low fluence Tb implanted ZnO crystals and annealing at 650 ^{o}C had no large effect on the Tb site location with 81% atoms still remain at substitutional lattice sites. TEM measurements showed that there is possibly a distribution in the Tb concentration. Disorder-induced peaks were observed in the Raman data after implantation and they were nearly suppressed after annealing at 650 ^{o}C. Superparamagnetic behavior was observed up to at least 300 K after annealing and it cannot be attributed to Tb, Tb_2O_3, or TbZn nanoparticles. It is possible that the superparamagnetism arises from defect clusters.

ACKNOWLEDGMENTS

We acknowledge funding from the Royal Society of New Zealand (VUW0917, 08-VUW-030), the Ministry of Science and Innovation (C05X0802, VICX0808) and the MacDiarmid Institute.

REFERENCES

1. S. A. Wolf, D. D. Awschalom, R. A. Buhrman, J. M. Daughton, S. von Molnr, M. L. Roukes, A. Y. Chtchelkanova, and D. M. Treger, *Science* **294**, 1488 (2001).
2. T. Dietl, H. Ohno, F. Matsukura, J. Cibert, and D. Ferrand, *Science* **287**, 1019 (2000).
3. F. Pan, C. Song, X. Liu, Y. Yang, and F. Zeng, *Mater. Sci. Eng. R.* **62**, 1 (2008).
4. S. Dhar, O. Brandt, M. Ramsteiner, V. F. Sapega, and K. H. Ploog, *Phys. Rev. Lett.* **94**, 037205 (2005).
5. K. Potzger, S. Zhou, F. Eichhorn, M. Helm, W. Skorupa, A. Mucklich, J. Fassbender, T. Herrmanns-Dorfer, and A. Bianchi, *J. Appl. Phys.* **99**, 063906 (2006).
6. J. Iqbal, X. Liu, H. Zhu, C. Pan, Y. Zhang, D. Yu, and R Yu, *J. Appl. Phys.* **106**, 083515 (2009).
7. M. Subramanian, P. Thakur, S. Gautam, K. H. Chae, M. Tanemura, T. Hihara, S. Vijayalakshmi, T. Soga, S. S. Kim, K Asokan, and R. Jayavel, *J. Phys. D: Appl. Phys.* **42**, 105410 (2009).
8. P. Photongkam, Y. B. Zhang, M. H. N. Assadi, S. Li, D. Yu, M. Ionescu, and A. V. Pan, *J. Appl. Phys.* **107**, 033909 (2010).
9. M. Ungureanu, H. Schmidt, H. von Wenckstern, H. Hochmuth, M. Lorenz, M. Grundmann, M. Fecioru-Morariu, G. Güntherodt, *Thin Solid Films* **515**, 8761 (2007).
10. P. P. Murmu, J. Kennedy, B. J. Ruck, G. V. M. Williams, A. Markwitz, S. Rubanov, and A. A. Suvorova, *J. Mater. Sci.* **47**, 1119 (2012).
11. S. Zhou, K. Potzger, A. Mucklich, F. Eichhorn, M. Helm, W. Skorupa, and J. Fassbender, *Nucl. Instrum. and Methods Phys. Res. B* **266**, 589 (2008).
12. Z. Wu, X. C. Liu, and J. C. A. Huang, *J. Mag. Mag. Mater.* **324**, 642 (2012).
13. J. Qi, Y. Yang, L. Zhang, J. Chi, D. Gao, and D. Xue, *Scr. Mater.***60**, 289 (2009).
14. V. Ney, S. Ye, T. Kammermeier, K. Ollefs, F. Wilhelm, A. Rogalev, S. Lebegue, A. L. da Rosa, and A. Ney, *Phys. Rev. B* **85**, 235203 (2012).
15. T. Monteiro, A. J. Neves, M. C. Carmo, M. J. Soares, M. Peres, E. Alves, E. Rita, and U. Wahl, *Superlatt. Microstruct.* **39**, 202 (2006).
16. A. Markwitz and J. Kennedy, *Int. J. Nano.* **6**, 369 (2009).
17. J. P. Biersack, *Nucl. Instrum. and Methods Phys. Res. B* **27**, 21 (1987).
18. J. Kennedy, A. Markwitz, H. J. Trodahl, B. J. Ruck, S. M. Durbin, and W. Gao, *J. Electron. Mater.* **36**, 472 (2007).
19. P. P. Murmu, R. J. Mendelsberg, J. Kennedy, D. A. Carder, B. J. Ruck, A. Markwitz, R. J. Reeves, P. Malar, and T. Osipowicz, *J. Appl. Phys.* **110**, 033534 (2011).
20. S. M. C. Miranda, M. Peres, T. Monteiro, E. Alves, H. D. Sun, T. Geruschke, R. Vianden, and K. Lorenz, *Optical Materials* **33**, 1139 (2011).
21. M. Schumm, M. Koerdel, S. Müller, H. Zutz, C. Ronning, J. Stehr, D.M. Hofmann, and J. Geurts, *New J. Phys.* **10**, 043004 (2008).
22. Z. Q. Chen, A. Kawasuso, Y. Xu, H. Naramoto, X. L. Yuan, T. Sekiguchi, R. Suzuki, and T. Ohdaira, *J. Appl. Phys.* **97**, 013528 (2005).
23. F. Friedrich and N. H. Nickel, *Appl. Phys. Lett.* **91**, 111903 (2007).
24. W. C. Thoburn, S. Legvold, and F. H. Spedding, *Phys. Rev.* **112**, 56 (1958).
25. B. C. Gerstein, F. J. Jelinek, and F. H. Spedding, *Phys. Rev. Lett.* **8**, 425 (1962).
26. J. B. MacChesney, H. J. Williams, R. C. Sherwood, and J. F. Potter, *J. Chem. Phys.* **44**, 596 (1966).
27. P. Morin, J. Rouchy, and E. du Tremolet de Lacheisserie, *Phys. Rev. B* **16**, 3182 (1977).
28. G. Z. Xing, Y. H. Lu, Y. F. Tian, J. B. Yi, C. C. Lim, Y. F. Li, G. P. Li, D. D. Wang, B. Yao, J. Ding, Y. P. Feng, and T. Wu, *AIP Adv.* **1**, 022152 (2011).
29. M. Khalid, M. Ziese, A. Setzer, P. Esquinazi, M. Lorenz, H. Hochmuth, M. Grundmann, D. Spemann, T. Butz, G. Brauer, et al., *Phys. Rev. B* **80**, 035331 (2009).
30. P. P. Murmu, J. Kennedy, G. V. M. Williams, B. J. Ruck, S. Granville, and S. V. Chong, *Appl. Phys. Lett.* **101**, 082408 (2012).